

# LocalNorm: Robust Image Classification through Dynamically Regularized Normalization

Bojian Yin<sup>1</sup> Siebren Schaafsma<sup>2</sup> Henk Corporaal<sup>3</sup> H. Steven Scholte<sup>4</sup> Sander M. Bohte<sup>1 5 6</sup>

## Abstract

While modern convolutional neural networks achieve outstanding accuracy on many image classification tasks, they are, compared to humans, much more sensitive to image degradation. Here, we describe a variant of Batch Normalization, LocalNorm, that regularizes the normalization layer in the spirit of Dropout while dynamically adapting to the local image intensity and contrast at test-time. We show that the resulting deep neural networks are much more resistant to noise-induced image degradation, improving accuracy by up to three times, while achieving the same or slightly better accuracy on non-degraded classical benchmarks. In computational terms, LocalNorm adds negligible training cost and little or no cost at inference time, and can be applied to already-trained networks in a straightforward manner.

## 1. Introduction

Methods that reduce internal covariate shift via learned rescaling and recentering neural activation, like Batch Normalization (Ioffe & Szegedy, 2015), have been an essential ingredient for successfully training deep neural networks (DNNs). In Batch Normalization, neural activation values are rescaled with trainable parameters, where summary neural activity is typically computed as mean and standard

<sup>1</sup>Machine Learning group, Centrum Wiskunde & Informatica (CWI), Amsterdam, The Netherlands <sup>2</sup>Holst Centre / IMEC, Eindhoven, The Netherlands <sup>3</sup>Dept of Electrical Engineering, Technical University Eindhoven, Eindhoven, The Netherlands <sup>4</sup>Dept of Psychology, University of Amsterdam, Amsterdam, The Netherlands <sup>5</sup>Dept of Biology, University of Amsterdam, Amsterdam, The Netherlands <sup>6</sup>Dept AI, Rijksuniversiteit Groningen, Groningen, The Netherlands. Correspondence to: Bojian Yin <Bojian.Yin@cwi.nl>, Sander Bohte <S.M.Bohte@cwi.nl>.

deviation over a batch of inputs. Such compact batch statistics however are sensitive to the input distribution, resulting in errors when novel images are outside this distribution, for example when faced with different and unseen lighting or noise conditions. Then, and unlike the human visual system, modern DNNs perform and generalize poorly (Geirhos et al., 2018).

While the original Batch Normalization computed statistics across the activity in a single feature map (or *channel*) (Ioffe & Szegedy, 2015), trainable normalizations have been proposed along a number of dimensions of deep neural network layers, including Layer Normalization, (Ba et al., 2016), Group Normalization (Wu & He, 2018), and Instance Normalization (Ulyanov et al., 2016); the recently proposed Switchable Normalization (Luo et al., 2018) meta-learns which normalization method to use during training. While these methods each have their merits, they do not resolve the sensitivity of DNNs to image-degradation because these have properties that are not observed by the network..

Here, we propose a local variant of Batch Normalization (BatchNorm), Local Normalization (LocalNorm), inspired by the continuous adaptation of spiking neurons to local temporal contrast (Mensi et al., 2016): we observe that the mean and variance in channel activity changes when images are subjected to noise-related degradation. Fig 1 shows an example of how the addition of Gaussian Noise flattens the

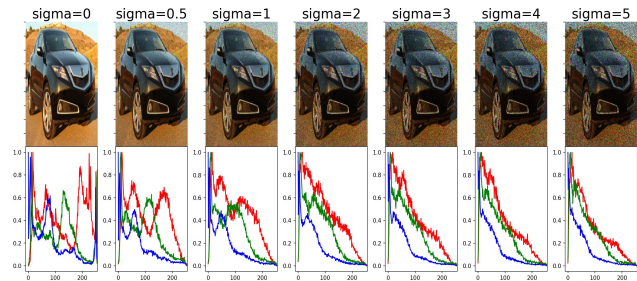


Figure 1. RGB-Histogram for increasing additive Gaussian noise



Figure 2. Examples of LocalNorm and BatchNorm classification on poorly lit or camouflaged images collected from the web.

color distribution for each channel in an image - other types of noise similarly affect the summary statistics, see Appendix. To increase the summary image statistical variance of the world from which the network learns, LocalNorm regularizes the normalization parameters during training by splitting the Batch into Groups, each with their own normalization scaling parameters. At test-time, the local channel statistics are then computed on the fly, either over a single image or a set (batch) of images in the test-set.

We show that DNNs trained with LocalNorm normalization are much more robust to image degradation: the trained networks exhibit strong performance for unseen images with noise conditions that are not in the training set. An example is shown in Figure 2, where poorly lit or camouflaged images of cars are misclassified in the network using BatchNorm and correctly classified by the same network architecture using LocalNorm. LocalNorm is straightforward to implement, also for networks already trained with standard BatchNorm - we show how a trained ResNet152 network trained further with LocalNorm improves accuracy for the Stanford Car dataset. Training networks from scratch, we show that LocalNorm achieves the same or slightly better performance as BatchNorm (and modern variants) on image

classification benchmarks at little additional computational expense.

## 2. Related work

Lighting and noise conditions can vary wildly over images, and various pre-processing steps are typically included in an image-processing pipeline to adjust color and reduce noise. In traditional computer vision, different filters and probabilistic models for image denoising are applied (Motwani et al., 2004). Modern approaches for noise removal include deep neural networks, like Noise2Noise (Lehtinen et al., 2018), DURR (Zhang et al., 2018b), and a denoising AutoEncoder (Vincent et al., 2010) where the network is trained on a combination of noisy and original images to improve its performance on noisy dataset thus increasing the networks’ robustness to image noise and also to train a better classifier. However, as noted in (Geirhos et al., 2018), training on images that include one type of noise in DNNs does not generalize to other types of noise.

### 2.1. Neural Normalizing techniques

Normalization is typically used to rescale the dynamic range of an image. This idea has also been applied to deep learn-

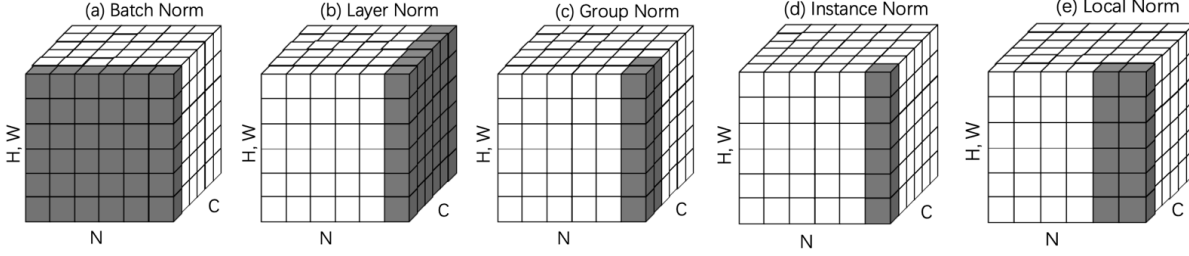


Figure 3. **Variants of Normalization Methods.** Each cube corresponds to a feature map tensor, with  $N$  as the batch axis,  $C$  as the channel axis, and  $(H, W)$  as the spatial axes – height and width. The pixels in gray are normalized by the same mean and variance, computed by aggregating the values of these pixels.

ing in various guises, and notably Batch Normalization (**BatchNorm**) (Ioffe & Szegedy, 2015) was introduced to renormalize the mean and standard deviation of neural activations using an end-to-end trainable parametrization.

**Normalization techniques.** A Normal-based normalization is generally computed as

$$\hat{x}_i = \frac{x_i - \mu_i}{\sigma_i + \epsilon} * \gamma + \beta$$

where the  $x_i$  is a part of feature tensor  $X = \{\cup x_i\}$  computed by the previous layer and  $\gamma$  and  $\beta$  are the (trainable) scaling parameters. For normal 3-Dimensional image like RGB and GBR,  $i = (i_N, i_W, i_H, i_C)$  is a 4D vector indexing the feature in  $[N, W, H, C]$  order where  $N$  is the batch size (number of images per batch),  $H$  and  $W$  are the spatial height and width axes, and  $C$  is the channel axis.

The space spanned by  $N, H, W, C$  can be subdivided and subsequently normalised in multiple ways. We call the subdivision, the elements on which this normalization is performed, a group  $G_k$ : different forms of input normalisations can be described as dealing with different groups. The mean  $\mu_k$  and standard deviation  $\sigma_k$  of the certain computation group  $G_k$  are computed as:

$$\mu_k = \frac{1}{m} \sum_{x_j \in G_k} x_j; \quad \sigma_k = \sqrt{\frac{1}{m} \sum_{x_j \in G_k} (x_j - \mu_i)^2 + \epsilon}$$

where  $\epsilon$  is a small constant like  $10^{-7}$ . The computation group  $G_k$  (where  $X = \{\cup G_k \mid k = 1, 2, \dots, K\}$ ) is a set of pixels which shares the mean  $\mu_k$  and std  $\sigma_k$ , and  $m$  is the size of the group  $G_k$ . BatchNorm and its variants can be mapped to a computational group along various axes

(Figure 3).

**Batch Normalization (BatchNorm)** was developed to ease training and improve convergence speed and generalization ability of deep neural networks. In 3(a), for each channel, BatchNorm computes  $\mu$  and  $\sigma$  along the  $(N, H, W)$  axes. The computational group of BatchNorm comprises of all the pixels (inputs) from all  $N$  batch samples sharing the same channel index. We can write this as  $G_k = \{p \mid p_c = i_c, c \in \{1, 2, 3, \dots, C\}\}$ , where  $p$  denotes the pixel and  $p_c$  the pixel’s channel index.

**Layer Normalization (LayerNorm)** (Ba et al., 2016) was designed to solve BatchNorm’s dependence on the batch size, and as a smart way to apply a normalization method on recurrent networks. LayerNorm estimates the statistical features of one sample, which could also correspond to an input of a time step in sequence inputs (Fig 3(b)). For each input sample, LayerNorm calculates ( $\mu$  and  $\sigma$ ) along the  $(H, W, C)$  axes: as for BatchNorm, the computational group of LayerNorm can be defined as  $G_k = \{p \mid p_n = i_n, n \in \{1, 2, 3, \dots, N\}\}$ .

**Group Normalization (GroupNorm)** (Wu & He, 2018) was designed to enable the use of larger batches. In general, the use of larger batch sizes improves the generalization ability of the network and accelerates the training process (Smith et al., 2017; Goyal et al., 2017). Large batch sizes however are typically limited by the locally available computational resources. Group normalization computes summarizing statistics only over a subset of channels (the group; Fig.3(c)), normalizing the computational group along the  $(H, W, C/K)$  axes. The computational group for GroupNorm is thus defined as  $G_k = \{p \mid p_n = i_n, \lfloor \frac{p_c}{C/K} \rfloor =$

$$\lfloor \frac{i_c}{C/K} \rfloor \}.$$

**Instance Normalization (InstaNorm)** (Ulyanov et al., 2016; 2017) was created for style transfer and quantity improvement. InstaNorm normalizes pixels of one sample in a single channel (Fig.3(d)). The InstaNorm computational group is defined as  $G_k = \{p | p_n = i_n, p_c = i_c, n \in \{1, 2, \dots, N\}, c \in \{1, 2, \dots, C\}\}$ .

**Switchable Normalization (SwitchNorm)** (Luo et al., 2018) was proposed as the linear combination of BatchNorm, LayerNorm and InstaNorm: in the SwitchNorm layer, the relative weighing of each kind of normalization method is adjusted during the training process. This allows the network to learn the right type of normalization at the right place in the network to improve performance; this does come however at the expense of a sizable increase in parameters and computation.

### 3. Local Normalization (LocalNorm)

We develop LocalNorm to improve the robustness of DNNs to various noise conditions. For BatchNorm, the mean  $\mu$  and std  $\sigma$  are calculated along all training samples in a channel and then fixed for evaluation on test images; as noted however, when the (test) image distribution changes, these statistical parameters will drift. As a result, DNNs with BatchNorm layers are sensitive to input that deviates from the training distribution, including noisy images.

Simply computing the summary statistics on-the-fly, to account for a potential drift, only partly solves the problem: in Figure 4, we show what happens when the mean  $\mu$  and std  $\sigma$  are computed as dynamical quantities also at test time for standard benchmarks CIFAR10 and Stanford Cars, using modern deep neural networks (for details, see below). For each test image (or batch of test images) we compute  $(\mu, \sigma)$ , for increasing noise (here for added Gaussian noise). For CIFAR10, Figure 4a, we find that using single test images when evaluating gives poor results, as the small (32x32) images do not result in channel activity sufficient for effective summarizing statistics; however, computing these statistics over a batch shows a marked improvement. Then, test accuracy exceeds standard BatchNorm for noisy images, at the expense of a slight decrease in accuracy for noiseless

images. For the large images in Stanford Cars, we see that dynamically computing  $(\mu, \sigma)$  at test time even for single images drastically improves accuracy (Fig 4b); the actual classification accuracy absent noise however drops. While computing summary statistics over a batch at test-time is feasible for benchmarking purposes, real world application would correspond to for example using a video stream, which would however substantially increase computational cost and latency.

In **LocalNorm**, we regularize the normalization layer for variations in  $\mu$  and  $\sigma$ . The aim is to make the trained architecture less sensitive to changes in these statistics at test-time, such that we can dynamically recompute  $\mu$  and  $\sigma$  on

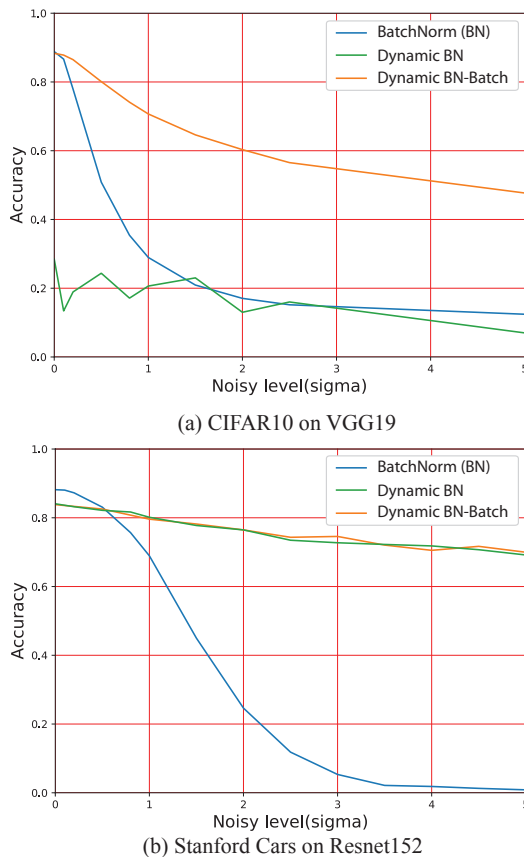


**Figure 4. AGN on CIFAR10 and Stanford Cars dataset.** Performance of a VGG19 network applied to Cifar10 (a) and a Resnet152 network to the Stanford Cars dataset (b) where the test-images are subjected to increasing amounts of image degradation, here in the form of Additive Gaussian Noise. Blue: accuracy for standard Batch Normalization. Orange: accuracy on dynamic Batch Normalization evaluated on single images. Green: accuracy on dynamic Batch Normalization with summary statistics computed over a batch of test-images.

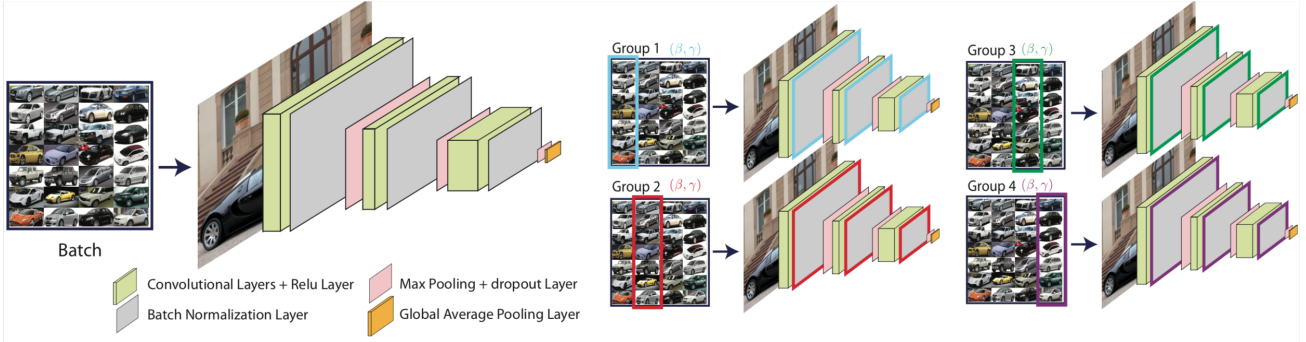


Figure 5. LocalNet. A deep network with standard batch normalization computes single summary statistics over the entire batch. In LocalNorm, summary statistics are computed over groups, where each group  $k$  is associated with its own scaling parameters  $\beta_k, \gamma_k$  (while sharing the all other network parameters), and summary statistics  $(\mu_k, \sigma_k)$  are dynamically computed also at test-time on the test-images.

test-images. We divide the Batch into separate Groups  $G_k$  for which we each compute summarizing statistics  $\mu_k, \sigma_k$  and associate separate scaling parameters  $\gamma_k$  and  $\beta_k$  with each Group (illustrated in Figure 5). As shown in Fig.3(e), for LocalNorm the computational group is defined along the  $(N/K, H, W)$  axes:

$$G_k = \left\{ p | p_c = i_c, \lfloor \frac{p_n}{N/K} \rfloor = \lfloor \frac{i_n}{N/K} \rfloor \right\}.$$

Effectively, each computational group can be regarded as a separate network sharing most parameters, where inputs are passed randomly through one such network during training.

As noted, for BatchNorm the channel summary statistics  $\mu, \sigma$  are taken as fixed from the training set after training. For LocalNorm, we recompute these statistics at test-time: this naturally incorporates changes in the image statistics, and the Group-induced regularized normalization ensures that the network also performs well for different such summary statistics.

Since LocalNorm provides both multiple independent Groups and computes summary statistics at test-time, there are different variants for classifying a novel image at test-time. Ideally, a single new image is passed through a randomly selected Group, such that summary statistics are computed on the fly only on this single image (SINGLE). A second method is to do the same, but pass a single image through all Groups and then use voting to determine the classification (SINGLE-VOTING). A third method is to collect the number of images corresponding to the Group size (VOTING), or use a set of images corresponding to the

Batch size (BATCH). For benchmark testing, BATCH is the fastest evaluation method, whereas SINGLE is the computationally most desirable method for real-world application. We use BATCH for all figures, and examine the different evaluation methods in detail in Section 5.3.

### 3.1. Implementation

LocalNorm is easily implemented in auto-differentiation frameworks like **Keras** (Chollet et al., 2015) and **Tensorflow** (Abadi et al., 2016) by adapting a standard batch normalization implementation<sup>1</sup>. For multi-GPUs, LocalNorm can map computational groups on separate GPUs which can accelerate training and allow the training of larger networks. In a variant of transfer learning (Pan et al., 2010), it is straightforward to adapt a model pre-trained with BatchNorm by replacing all BatchNorm layers with LocalNorm layers initialized with the BatchNorm parameters, and then continue training.

## 4. Image Noise

We test LocalNorm in a Noisy-object classification task where synthetic Gaussian, Poisson and Bernoulli noise is added to images, as in Noise2Noise (Lehtinen et al., 2018). All three kinds of independent noise  $\xi$  are added on each channel of the image  $x_c$  as follows:

For **Additive Gaussian Noise (AGN)**, Gaussian noise with zero mean is added to the image on each channel, defined as  $\hat{x}_c = x_c(1 + \xi), \xi \sim \text{Gaussian}(0, \sigma_n)$ .

<sup>1</sup>code available at <https://github.com/byin-cwi/LocalNorm1>

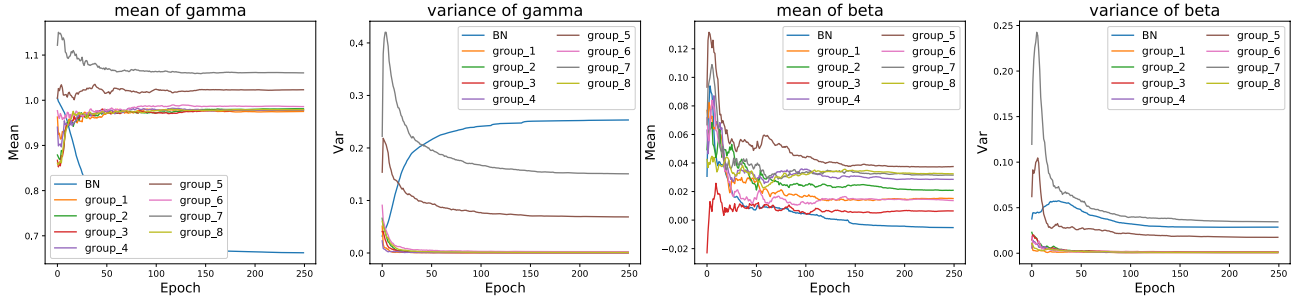


Figure 6. Development of mean and variance of the scaling parameters  $\gamma$  and  $\beta$  for LocalNorm Groups (group\_x) and BatchNorm (BN) during training on CIFAR10.

**Additive Poisson Noise (APN)** is one of the most dominating noise sources in photographs, and is easily visible in low-light images. APN is a type of zero-mean noise and is hard to remove by pre-processing because it is distributed independently at each channel. Mathematically, APN is computed as  $\hat{x}_c = x_c + 255\xi$  or  $\hat{x}_c = x_c(1 + \xi)$   $\xi \sim Poisson(0, \sigma_n)$ , where  $\sigma_n \in [0, 1]$ .

**Multiplicative Bernoulli Noise (MBN)** removes some random pixels from the image with probability  $\sigma_n$ . MBN defined by  $\hat{x} = x\xi, \xi \sim Bernoulli(\sigma_n)$ .

## 5. Experimental Results

### 5.1. Benchmark Accuracy

We apply LocalNorm to a number of classical benchmarks: MNIST (LeCun et al., 1998), CIFAR10 (Krizhevsky & Hinton, 2009), and Stanford Cars (Krause et al., 2013), and compare with other normalization methods. Results are shown in Table 1: using otherwise identical network architectures, all three normalization methods achieve near state-of-the-art accuracy on the original datasets, where in 3 out of 4 cases, LocalNorm slightly outperforms BatchNorm and SwitchNorm. Comparing training time, for CIFAR10, we find that LocalNorm incurs only a small computational cost (10-20%), while SwitchNorm proves much more computationally expensive (Table 1).

For MNIST, we designed a standard DNN (Input-16c-16c-32c-32c-512d-1024d-output), we set the batch size to 100; for LocalNorm, we divide the batch into 10 computational groups with 10 images each group. For CIFAR10, we use two classical network architectures – VGG19 and ResNet32. The classical **VGG19** network architecture (Simonyan &

Zisserman, 2014) is often used as a baseline to test new network architectures. **Residual Networks, or ResNets** (He et al., 2016) have achieved state-of-the-art accuracy on many machine learning datasets, and ResNet32 (a ResNet with 32 Layers) achieves competitive results on the CIFAR10 dataset (Zhang et al., 2018a). We use a batch size of 128, as in most recent state-of-the-art models. For LocalNorm, we divide the batch into 8 computational groups with 16 images per group by default.

	MNIST	CIFAR10-VGG	CIFAR10-ResNet	Stanford-Car
<b>BatchNorm</b>	99.61%	88.83%	91.74%	88.17%
<b>SwitchNorm</b>	99.53%	57.39%	<b>91.88%</b>	87.34%
<b>LocalNorm</b>	<b>99.62%</b>	<b>92.07%</b>	91.78%	<b>89.34%</b>

Table 1. The accuracy on original test dataset of each network with various types of normalization on each dataset

Models	VGG19		ResNet32	
	Speed (s/epoch)	Paras	Speed (s/epoch)	Paras
<b>BatchNorm</b>	20s	15,001,418	21s	470,218
<b>LocalNorm</b>	23s	15,115,690	26s	473,610
<b>SwitchNorm</b>	30s	15,001,496	56s	470,414

Table 2. Training speed and model size on VGG19 and ResNet32 with various Norms on CIFAR10 on an Nvidia Titan Xp.

The Stanford Cars dataset contains 16,185 images of 196 classes of cars, and each image is large, similar to images in the ImageNet dataset, allowing us to compare LocalNorm to the other normalization methods when applied to large networks and large images. The training and test dataset are similarly large, and the images are taken under various conditions. We use ResNet152 for this dataset for improved accuracy; 16 images are trained as a batch and are divided into 4 groups for LocalNorm. For ResNet152, we use the pre-trained ImageNet weights from github<sup>2</sup> and then continue training this network with BatchNorm, SwitchNorm

<sup>2</sup><https://gist.github.com/flyyufelix/7e2eafb149f72f4d38dd661882c554a6>

or LocalNorm.

In Figure 6 we plot the development of mean and variance of the normalization scaling parameters  $\gamma$  and  $\beta$  for LocalNorm and BatchNorm (averaged over all channels) when training VGG19 on CIFAR10 using 8 Groups for LocalNorm. We see that LocalNorm converges to a spread of  $\gamma$  and  $\beta$  values during training.

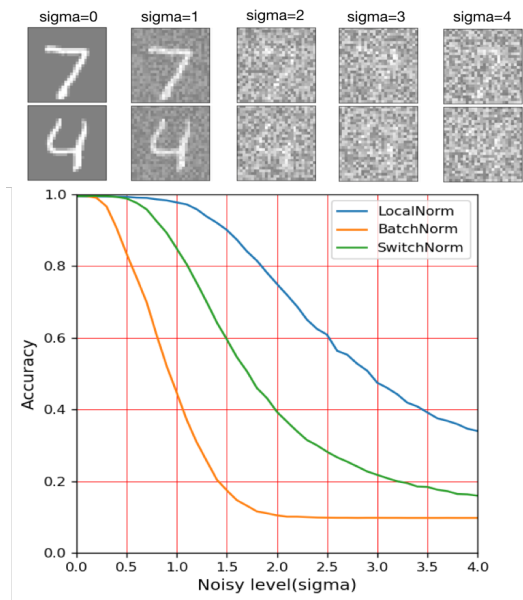


Figure 7. **MNIST accuracy and noisy image.** The top row shows the image quality under different AGN, and Line graph plots the accuracy obtained for noise-degraded digits.

## 5.2. Noisy Image degradation

To measure noise robustness and noise generalization, we use the networks trained with various normalization methods and the original training dataset, and test them on images degraded with different levels of noise.

**MNIST** In the MNIST dataset, images only have one channel. We apply AGN to MNIST to demonstrate DNN performance facing out-of-sample noise-degraded images. In Fig 7, we see that for all normalization methods, performance decreases when images become more degraded, e.g., for  $\sigma_n = 1$ , the digit is clearly visible as is some noise. The performance of BatchNorm and SwitchNorm however decreases to 44.67% and 84.89% respectively, while LocalNorm still achieved an accuracy of over 90% with **97.78%**; for  $\sigma_n = 2$ , where BatchNorm already yields random choice

performance (around 10%), LocalNorm still performs with moderately reduced accuracy of 75.01% (SwitchNorm obtains 39.31%). For very high noise levels, also difficult for humans, LocalNorm still outperforms SwitchNorm by a factor of two.

**CIFAR10** We tested VGG19 trained on CIFAR10 with various normalization methods on noisy test images degraded with AGN. Figure 8a shows that the accuracy when using BatchNorm decreases rapidly, achieving only 28.95% accuracy for sigma=1; for the same noise level, the LocalNorm network performs over twice as well at 71.95% accuracy. Similar observations apply for the other types of noise. For APN, both BatchNorm and LocalNorm’s accuracy curve dropped sharply, while the LocalNorm still substantially outperforms BatchNorm and SwitchNorm in general (Fig 8b). For MBN in Figure 8c, both SwitchNorm and BatchNorm’s accuracy drops exponentially and converge to random choice, while LocalNorm’s performance decreases slower. We see the same performance order for a ResNet32 network applied to CIFAR10 (see Appendix, Figure 14).

**Stanford Car Dataset** For the large images in the Stanford Cars dataset, we find that when testing on noisy images (Fig.8d), LocalNorm maintains a test accuracy over 74% under any tested level of AGN, while under BatchNorm accuracy declines sharply to < 20% for sigma > 2.5; a similar behavior is observed for APN (Fig 8e). For MBN, Figure 8f, the BatchNorm accuracy decreases exponentially while LocalNorm’s performance declines essentially linearly<sup>3</sup>.

To directly investigate generalization ability under different noise levels, we computed the confusion matrix for each model under various conditions: this is shown in Figures 15-17 in the Appendix. In general, we find that networks using BatchNorm increasingly default classification to a select few classes for increasing noise levels, whereas for networks using LocalNorm this is not the case - classification becomes essentially random.

<sup>3</sup>For Stanford Cars, we omitted data for SN as we obtained near-zero performance on noise-degraded images with the publicly available code.

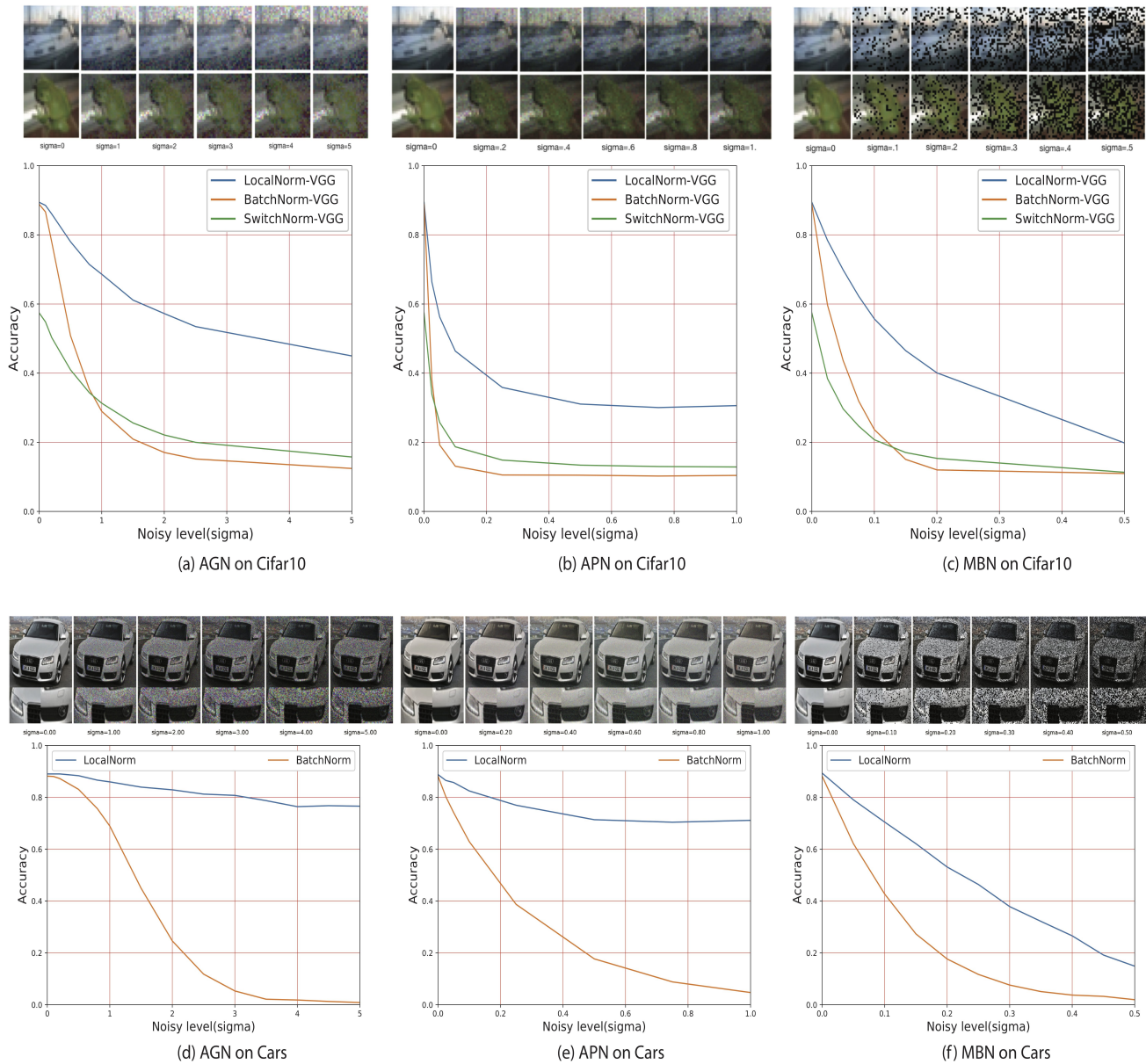
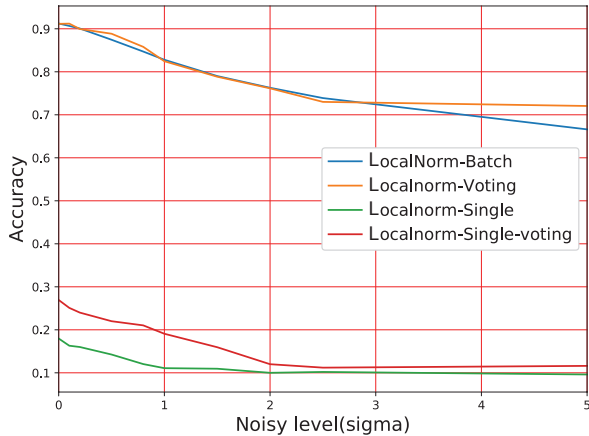


Figure 8. Noise effect on CIFAR10 (a-c) and Stanford Cars datasets (d-f). (a-c) Top row illustrates noise-degraded CIFAR10 images for different amounts of AGN, AGN and MBN respectively. Bottom row, line graphs plot corresponding network accuracy on degraded CIFAR10 images using a VGG19 network architecture; (d-f) same noise-degradations applied to the Stanford Cars images using a ResNet152 network architecture.

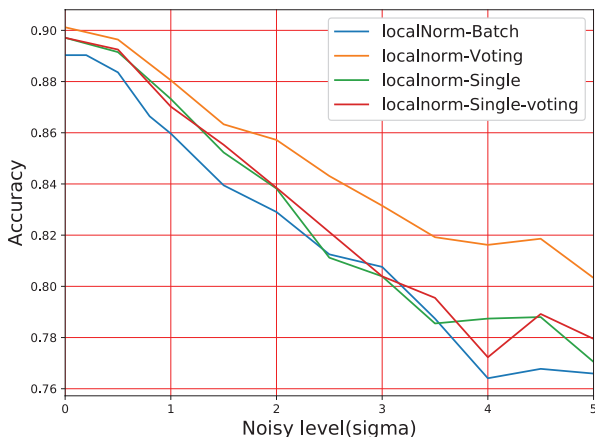
### 5.3. Evaluation Methods

We evaluated all benchmarks using the BATCH evaluation method. This is fast and demonstrates performance when a set of images equal to the Group size is evaluated in a randomly selected Group. For evaluating a single image at test-time, the other methods are more desirable, in particular SINGLE and SINGLE-VOTING. In Figure 9, we examine the various evaluation methods for AGN in CIFAR10 and

Stanford Cars (results hold for APN and MBN as well, not shown). We find that SINGLE-VOTING and SINGLE are feasible for Stanford Cars (Fig. 9b), where VOTING achieves the highest accuracy in noisy conditions, likely as it both captures the summary statistics best and averages over the Groups. With LocalNorm, compared to the dynamical BatchNorm examined in Figure 4b, performance on the original noiseless test-set now exceeds that of BatchNorm.



(a) CIFAR10 evaluation



(b) Cars evaluation

Figure 9. LocalNorm performance for various evaluation methods on CIFAR10 (a) and Stanford Cars dataset (b) under AGN

For CIFAR10 (Fig. 9b), we find that more images are needed to capture the summarizing statistics at test-time: only VOTING and BATCH perform well, with VOTING being slightly more robust than BATCH. Again, with LocalNorm accuracy on the noiseless test-set now exceeds BatchNorm. Additionally, compared to the dynamical batch version of BatchNorm, LocalNorm is much more robust to noisy images. The interpretation for the inability to use single images for evaluation for CIFAR10 (and also for MNIST, not shown) is straightforward: for the large images in Stanford Cars, a single image provides sufficient statistics, whereas for the small images in CIFAR10, a set of images is needed.

#### 5.4. Training effects

**Training on augmented noisy datasets.** We next examine

how network robustness improves when noisy AGN images are added to the *training* dataset. As can be seen in Figure 10, when testing on images with AGN or MBN noise, adding AGN noise samples in the training set does improve accuracy for BatchNorm-trained networks on noisy test-images. This AGN-noise network however hardly improves accuracy on test-data containing Poisson noise (APN) or Bernoulli noise (MBN), confirming the observation in (Geirhos et al., 2018) that noise is hard to generalize. Moreover, networks trained using LocalNorm without added noise samples still perform better, and we also find that for the noise-augmented BatchNorm network the test accuracy on the original dataset is slightly reduced. In practice, it is next to impossible to cover all noise conditions in the training dataset, and training with many such added examples is computationally expensive.

**Group size.** LocalNorm has as a parameter the number of groups which, for a given batch size, determines the number of images in each group. While we did not extensively optimize for group number, we found that a small-ish number of groups, 4-8, performed best in practice for the batch sizes used in this study (Fig 11).

## 6. Conclusion

Here, we develop an effective and robust normalization layer—LocalNorm. LocalNorm regularizes the Normalization layer during training, and includes a dynamic computation of the Normalization layer’s summary statistics during test-time. The key insight here is that out-of-sample conditions, like noise degradation, will shift the summary statistics of an image, and the LocalNorm approach makes a DNN more robust to such shifts.

We demonstrate the effectiveness of the approach on classical benchmarks, including both small and large images, and find that LocalNorm decisively outperforms both classical Batch Normalization and modern variants like SwitchNorm. We show that computing LocalNorm only has a limited computational cost with respect to training time, of order 10-20%. LocalNorm furthermore can be evaluated on batches of test-images, and, for large enough images, also on single images passed through only a single group, then incurring the same evaluation cost as Batch Normalization. The ef-

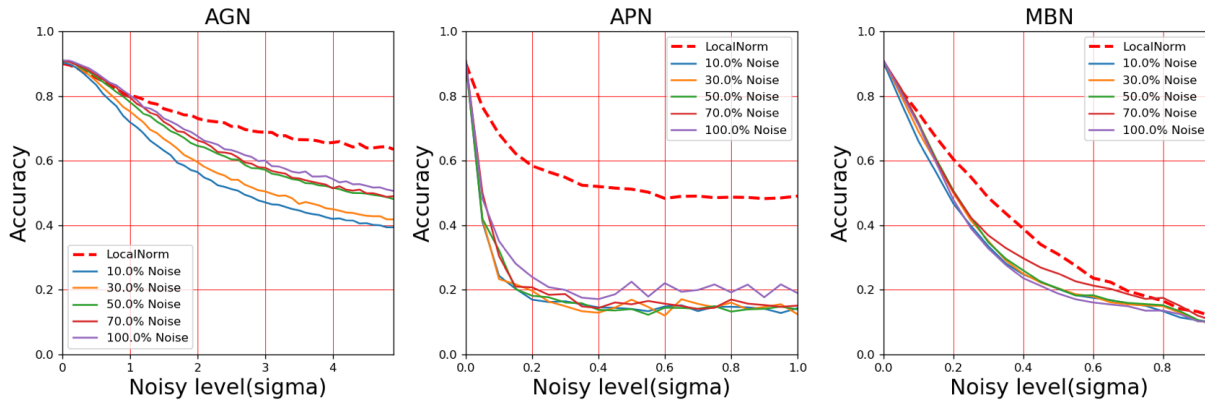


Figure 10. Training ResNet32 on a training set augmented with an increasing number of AGN images in CIFAR10, for sigma=1.

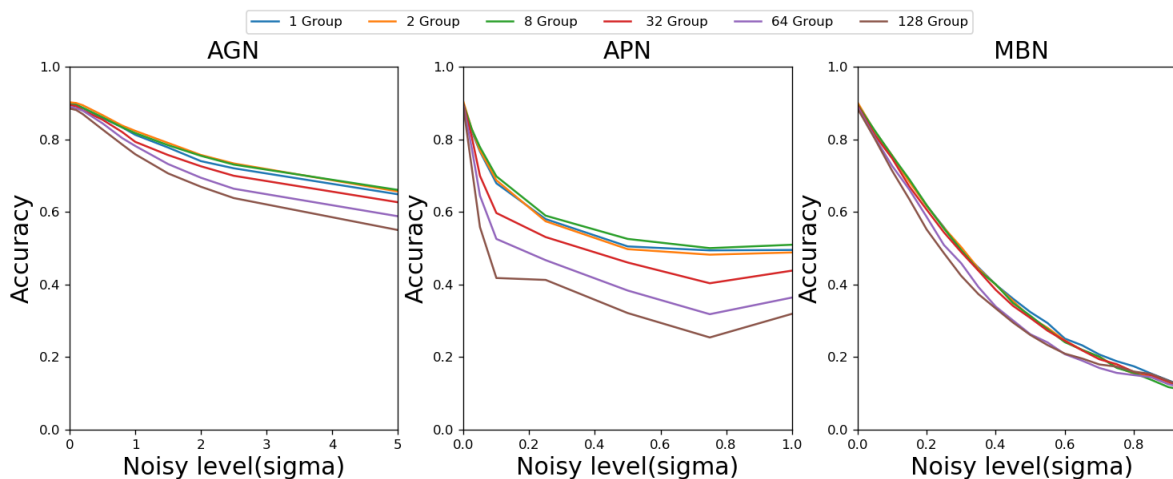


Figure 11. Group number’s influence on LocalNorm performance on Cifar10 (using VGG19)

fectiveness of Batch evaluation suggests that LocalNorm could be applied to a brief stream of images, capturing both the local (in time) image statistics and allow averaging over multiple views of the same object.

**Acknowledgments**

BY is funded by the NWO-TTW Programme “Efficient Deep Learning” (EDL); the Titan Xp used for this research was donated by the NVIDIA Corporation.

**References**

Abadi, M., Barham, P., Chen, J., Chen, Z., Davis, A., Dean, J., Devin, M., Ghemawat, S., Irving, G., Isard, M., et al. Tensorflow: a system for large-scale machine learning. In *OSDI*, volume 16, pp. 265–283, 2016.

Ba, J. L., Kiros, J. R., and Hinton, G. E. Layer normalization. *arXiv preprint arXiv:1607.06450*, 2016.

Chollet, F. et al. Keras. <https://github.com/fchollet/keras>, 2015.

Geirhos, R., Temme, C. R., Rauber, J., Schütt, H. H., Bethge, M., and Wichmann, F. A. Generalisation in humans and deep neural networks. In *Advances in Neural Information Processing Systems*, pp. 7549–7561, 2018.

Goyal, P., Dollár, P., Girshick, R. B., Noordhuis, P., Wesolowski, L., Kyrola, A., Tulloch, A., Jia, Y., and He, K. Accurate, large minibatch SGD: training imagenet in 1 hour. *CoRR*, abs/1706.02677, 2017. URL <http://arxiv.org/abs/1706.02677>.

He, K., Zhang, X., Ren, S., and Sun, J. Deep residual learn-

- ing for image recognition. In *Proceedings of the IEEE conference on computer vision and pattern recognition*, pp. 770–778, 2016.
- Ioffe, S. and Szegedy, C. Batch normalization: Accelerating deep network training by reducing internal covariate shift. *arXiv preprint arXiv:1502.03167*, 2015.
- Krause, J., Stark, M., Deng, J., and Fei-Fei, L. 3d object representations for fine-grained categorization. In *4th International IEEE Workshop on 3D Representation and Recognition (3dRR-13)*, Sydney, Australia, 2013.
- Krizhevsky, A. and Hinton, G. Learning multiple layers of features from tiny images. Technical report, Citeseer, 2009.
- LeCun, Y., Bottou, L., Bengio, Y., and Haffner, P. Gradient-based learning applied to document recognition. *Proceedings of the IEEE*, 86(11):2278–2324, 1998.
- Lehtinen, J., Munkberg, J., Hasselgren, J., Laine, S., Karras, T., Aittala, M., and Aila, T. Noise2noise: Learning image restoration without clean data. *CoRR*, abs/1803.04189, 2018. URL <http://arxiv.org/abs/1803.04189>.
- Luo, P., Ren, J., and Peng, Z. Differentiable learning-to-normalize via switchable normalization. *arXiv preprint arXiv:1806.10779*, 2018.
- Mensi, S., Hagens, O., Gerstner, W., and Pozzorini, C. Enhanced sensitivity to rapid input fluctuations by nonlinear threshold dynamics in neocortical pyramidal neurons. *PLoS Comput. Biol.*, 12(2):e1004761, February 2016.
- Motwani, M. C., Gadiya, M. C., Motwani, R. C., and Harris, F. C. Survey of image denoising techniques. In *Proceedings of GSPX*, pp. 27–30, 2004.
- Pan, S. J., Yang, Q., et al. A survey on transfer learning. *IEEE Transactions on knowledge and data engineering*, 22(10):1345–1359, 2010.
- Simonyan, K. and Zisserman, A. Very deep convolutional networks for large-scale image recognition. *CoRR*, abs/1409.1556, 2014. URL <http://arxiv.org/abs/1409.1556>.
- Smith, S. L., Kindermans, P., and Le, Q. V. Don’t decay the learning rate, increase the batch size. *CoRR*, abs/1711.00489, 2017. URL <http://arxiv.org/abs/1711.00489>.
- Ulyanov, D., Vedaldi, A., and Lempitsky, V. S. Instance normalization: The missing ingredient for fast stylization. *CoRR*, abs/1607.08022, 2016. URL <http://arxiv.org/abs/1607.08022>.
- Ulyanov, D., Vedaldi, A., and Lempitsky, V. S. Improved texture networks: Maximizing quality and diversity in feed-forward stylization and texture synthesis. *CoRR*, abs/1701.02096, 2017. URL <http://arxiv.org/abs/1701.02096>.
- Vincent, P., Larochelle, H., Lajoie, I., Bengio, Y., and Manzagol, P.-A. Stacked denoising autoencoders: Learning useful representations in a deep network with a local denoising criterion. *Journal of machine learning research*, 11(Dec):3371–3408, 2010.
- Wu, Y. and He, K. Group normalization. *arXiv preprint arXiv:1803.08494*, 2018.
- Zhang, G., Wang, C., Xu, B., and Grosse, R. Three mechanisms of weight decay regularization. *arXiv preprint arXiv:1810.12281*, 2018a.
- Zhang, X., Lu, Y., Liu, J., and Dong, B. Dynamically unfolding recurrent restorer: A moving endpoint control method for image restoration. *CoRR*, abs/1805.07709, 2018b. URL <http://arxiv.org/abs/1805.07709>.

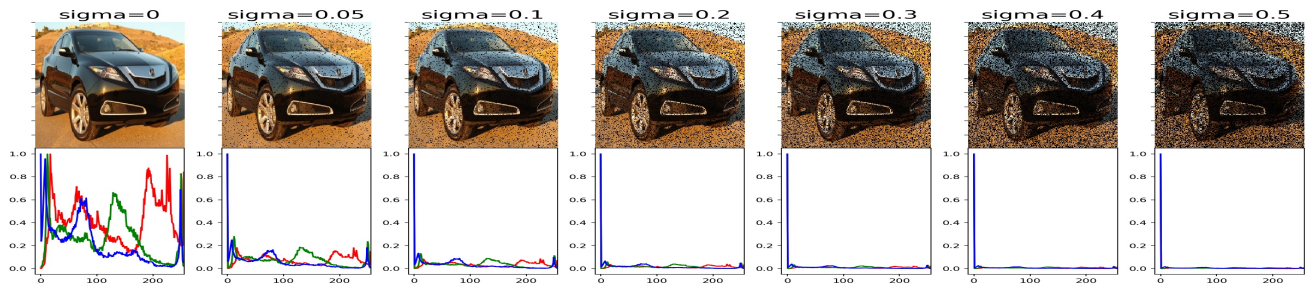


Figure 12. RGB-Histogram for MBN-type noise.

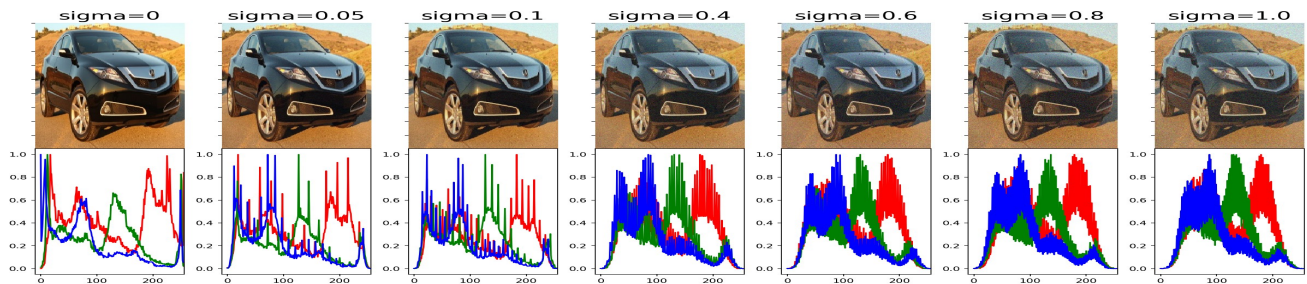


Figure 13. RGB-Histogram for APN-type noise.

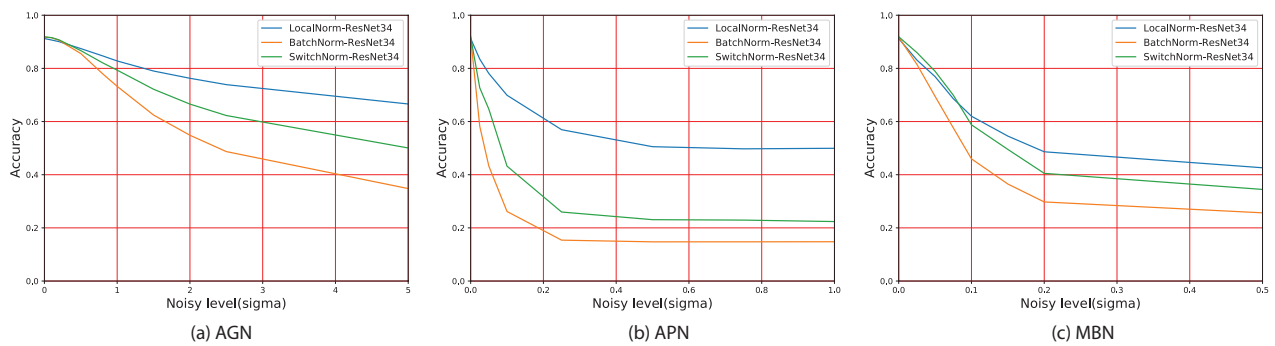


Figure 14. ResNet32 on CIFAR10

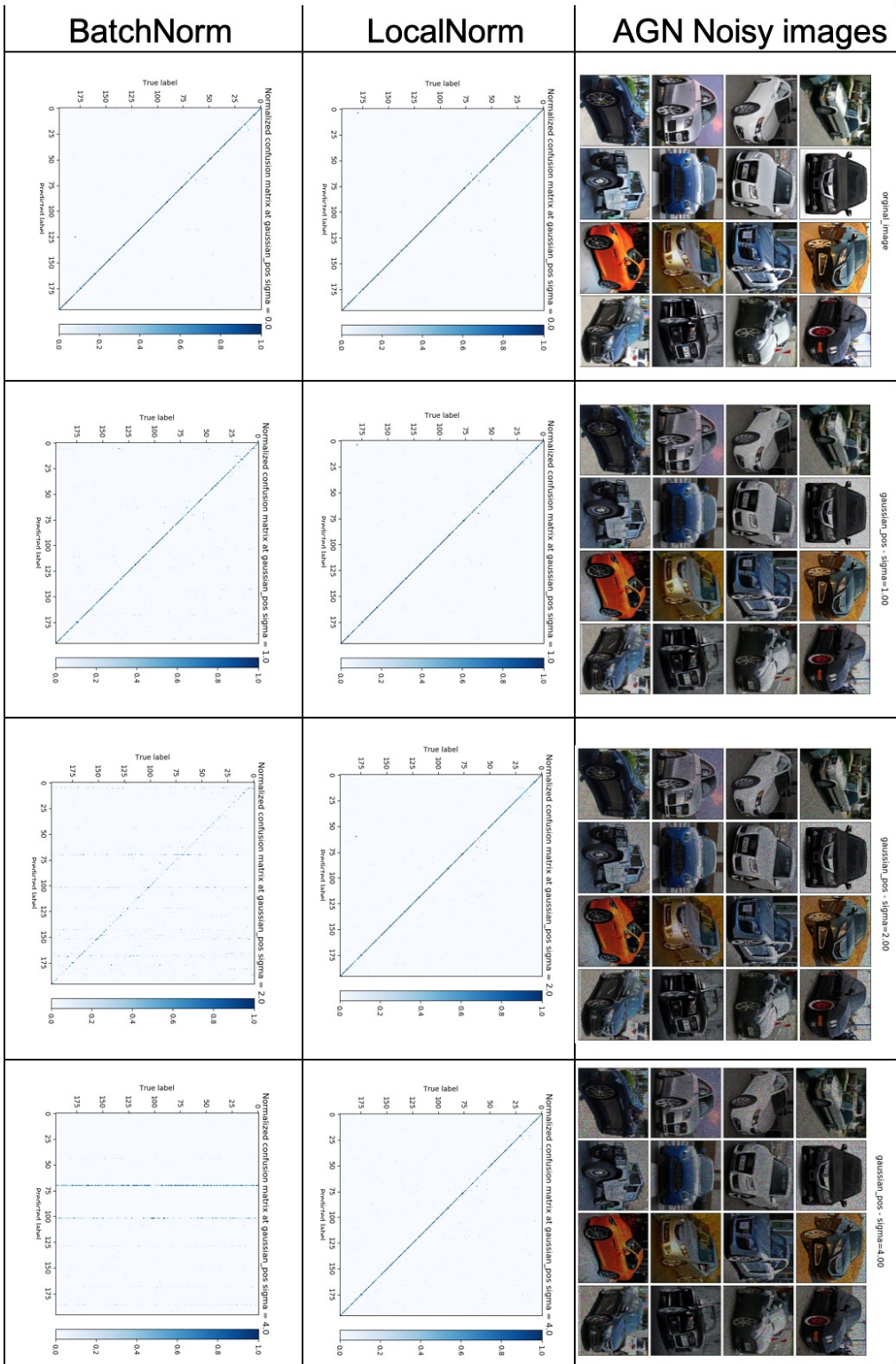


Figure 15. Confusion matrix under AGN noise for  $\sigma = \{0, 1, 2, 4\}$

# LocalNorm: Robust Image Classification through Dynamically Regularized Normalization

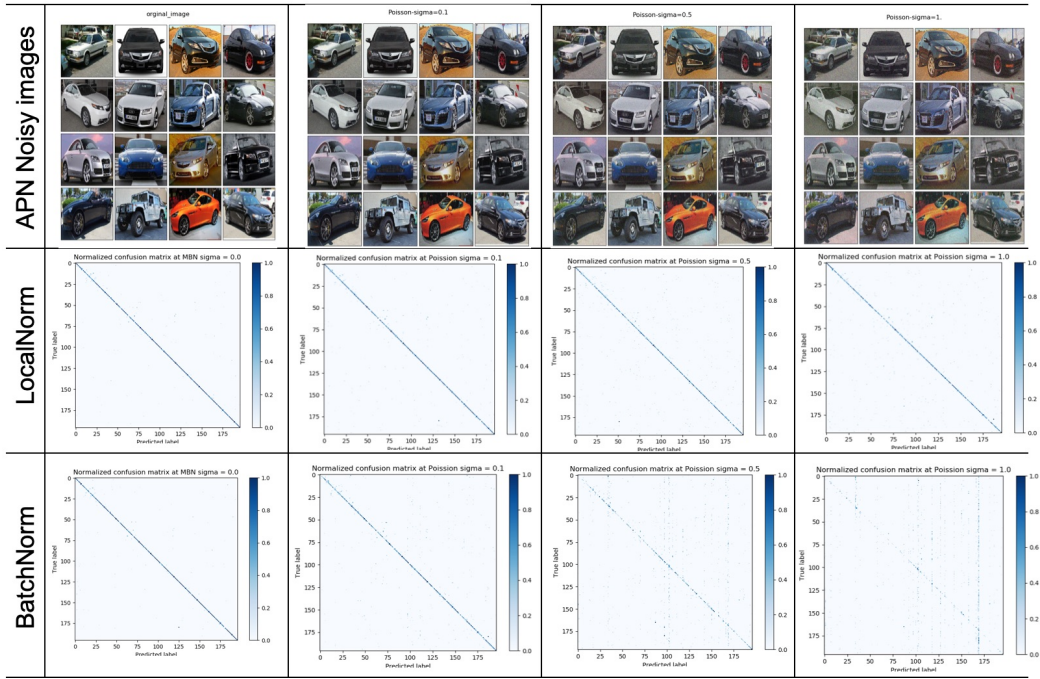


Figure 16. Confusion matrix under APN noise where  $\sigma = \{0, .1, .5, 1.\}$

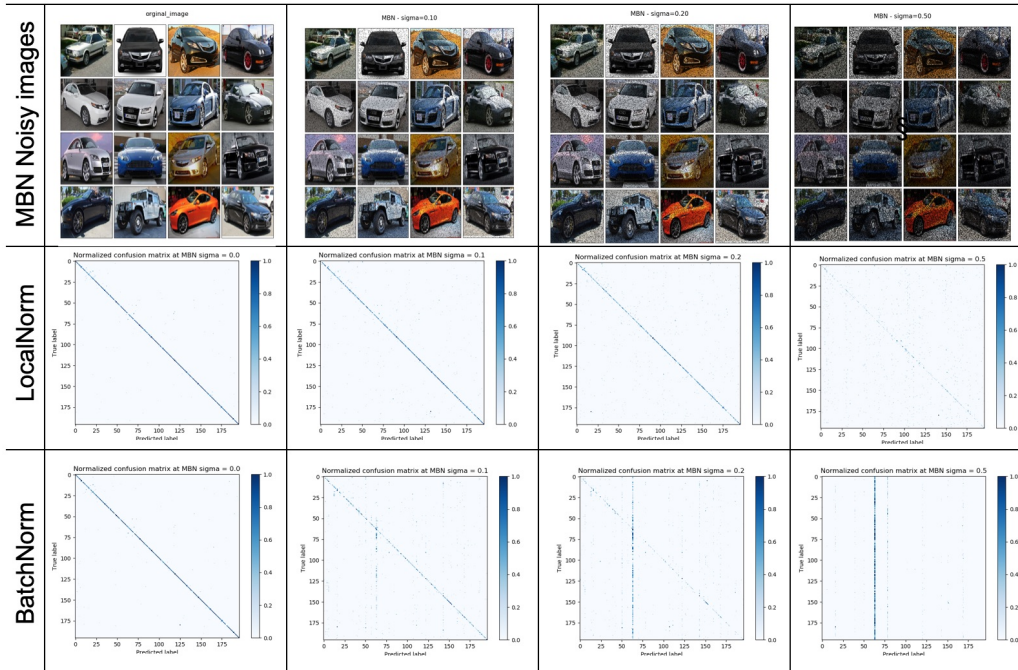


Figure 17. Confusion matrix under MBN noise where  $\sigma = \{0, .1, .2, .5\}$